PERGAMON

International Journal of Heat and Mass Transfer 43 (2000) 2841–2857

International Journal of HEAT and MASS TRANSFER

www.elsevier.com/locate/ijhmt

Impact, recoil and splashing of molten metal droplets

Shiraz D. Aziz, Sanjeev Chandra*

Department of Mechanical and Industrial Engineering, University of Toronto, 5 King's College Road, Toronto, Ont., Canada M5S 3G8

Received 23 June 1999; received in revised form 1 November 1999

Abstract

We studied the impact and solidification of molten tin droplets on a stainless steel surface. Droplet impact velocity was varied from 1.0 to 4.0 m/s and substrate temperature from 25 to 240°C (above the melting point of tin, 232°C). We photographed droplet impact and measured splat diameter and liquid–solid contact angle from these photographs. Substrate temperature under an impacting droplet was measured using a fast response thermocouple. Thermal contact resistance at the droplet–substrate interface was calculated by matching measured surface temperature variation with an analytical solution. A simple energy conservation model was used to predict the maximum spread of droplets during impact. Predictions agreed well with measured values. Instabilities were observed on the periphery of the droplet, which led to the formation of fingers. A model based on the Rayleigh–Taylor instability was used to predict the number of fingers around the periphery of the droplet.

Keywords: Droplet impact; Rapid solidification; Spray watering; Droplet splashing; Metal droplets

1. Introduction

The impact of a liquid droplet on a solid surface is a fascinating phenomenon. Worthington [1] was the first to photograph water droplets as they impinged on a solid surface, revealing the complex shapes that droplets assume as they spread and splash during impact. Since then there has been much effort devoted to studies of droplet impact, motivated by the development of several technologies that involve deposition of liquid droplets on solid surfaces. Applications in which droplet impact models have been used include spray cooling of hot surfaces, ink jet printing, spray painting, fire suppression using sprinkler systems, spray forming, deposition of solder bumps on printed circuit boards, thermal spray coating, soil erosion by rain drops, and ice accumulation on electric wires and aircraft. From a researcher's viewpoint, analysis of droplet impact and splashing offers very interesting challenges. Much of the physical phenomena involved is poorly understood, including flow of free liquid surfaces, motion of a liquid–solid–air contact line, wetting of solid surfaces, and fluid instabilities that cause formation of fingers around the droplet periphery, leading to detachment of satellite droplets. The problem becomes even more complex if droplets freeze while spreading.

Our research into the impact and spreading of molten metal droplets on a solid surface is part of a larger study of thermal spray coating. This is an industrial process in which metal or ceramic powders are injected into a high temperature gas jet

* Corresponding author: Tel.: +1-416-978-5742; fax: +1-416-978-7753.

E-mail address: chandra@mie.utoronto.ca (S. Chandra).

0017-9310/00/$ - see front matter
PII: S0017-9310(99)00350-6

Nomenclature

a	acceleration of liquid–air interface
C	specific heat
d_s	diameter of solid layer
D	splat diameter, measured at the splat–substrate interface
D_o	diameter of spherical droplet
D_{max}	maximum splat diameter
H_f	latent heat of fusion
k	thermal conductivity
K	splash parameter ($= \sqrt{We\sqrt{Re}}$)
KE_1	initial kinetic energy
ΔKE	kinetic energy loss due to solidification
N	number of fingers
R_c	thermal contact resistance
s	thickness of solid layer
s^*	dimensionless thickness of solid layer ($= s/D_o$)
SE_1	droplet surface energy before impact
SE_2	droplet surface energy after impact
t	time
t^*	dimensionless time ($= V_o t/D_o$)
t_c^*	dimensionless time for droplet to reach its maximum spread diameter
T_d	droplet temperature
T_m	droplet melting temperature
T_w	substrate temperature
$T_{w,i}$	initial substrate temperature
ΔT	increase in surface temperature ($= T_w - T_{w,i}$)
ΔT_{max}	maximum increase in surface temperature
V	velocity
V_o	droplet impact velocity
W	work done in deforming droplet

Greek symbols

α	thermal diffusivity
γ	$= k\rho C$
σ	surface tension
λ	wavelength
μ	viscosity
ν	kinematic viscosity
ρ	density
θ	liquid–solid contact angle
θ_a	advancing contact angle
Φ	solidification parameter
ξ	spread factor ($= D/D_o$)
ξ_{max}	maximum spread factor
ψ_{SE_2}	normalised surface energy
ψ_w	normalised viscous energy dissipation
$\psi_{\Delta KE}$	normalised kinetic energy loss due to solidification

Dimensionless numbers

Bi	Biot number ($= D_o/(R_c k_d)$)
Pe	Peclet number ($= V_o D_o/\alpha$)
Pr	Prandtl number ($= \nu/\alpha$)
Re	Reynolds number ($= V_o D_o/\nu$)
Ste	Stefan number ($= C(T_m - T_{w,i})/H_f$)
We	Weber number ($= \rho V_o^2 D_o/\sigma$)

Subscripts

d	droplet
w	substrate

produced by either striking an electric arc or burning a fuel, where they melt while being accelerated towards the surface to be coated. Molten droplets rapidly solidify when they impact on the substrate, producing dense deposits with fine-grained, homogeneous microstructures. Thermal sprayed coatings are widely used to protect components exposed to corrosion, wear or heat. The mechanical properties of coatings are known [2] to depend strongly on the shape of splats formed by individual droplets as they impact and freeze. An understanding of the fundamental physical principles governing droplet impact and solidification is essential to determining the relation between process parameters (such as gas velocity, gas temperature, substrate temperature, substrate thermophysical properties, powder size, and powder material) and the structure of coatings.

To illustrate the variety of phenomena that we wish to analyse, Fig. 1 shows micrographs of splats formed during plasma spraying. They were formed by depositing nickel powder (mean particle diameter 61 μm, standard deviation 9 μm) with an average velocity of 48 m/s and temperature of 2050°C onto (a) a glass surface at 356°C, and (b) a polished stainless steel surface at 368°C. Details of how these samples were obtained have been given elsewhere [3]. In each picture two splats are visible, one partially covering the other. Splats on steel were smaller than those on glass and did not flatten out completely, suggesting freezing arrested their motion before spreading was complete. In both cases only the second droplet showed evidence of splashing, perhaps because of a fluid instability triggered by contact with the edge of the previously deposited splat. Splashing and incomplete flattening both degrade coating quality since they leave voids in the deposit, increasing its porosity and reducing its

strength. It is therefore important to understand the effect of droplet and substrate properties on splat shape.

Relatively few experimental studies have been done to examine molten metal droplet impact. Madejski [4] developed a simple model that predicted the maximum extent of spread of a molten droplet impacting on a solid surface, which agreed—within an order of magnitude—with the size of splats formed by dropping tin and lead droplets on a flat plate. Inada [5] measured the temperature variation of a copper surface on which a lead drop was dropped, and estimated the surface heat flux. Inada and Yang [6] photographed the underside of a lead droplet as it landed on a quartz plate and observed solidification at the droplet–substrate interface. Collings et al. [7] dropped molten alloy droplets on surfaces of copper, alumina and quartz, and found that the splat shape depended on substrate thermal properties. Fukanuma and Ohmori [8] photographed the impact of superheated tin and zinc droplets on a cold stainless steel plate, and discovered that droplets solidified after spreading. Watanabe et al. [9] released alkane droplets onto a surface maintained at below their freezing point, and also concluded that solidification was too slow to affect droplet spread. Schiffiano and Sonin [10,11] studied impact of molten droplets on a surface at low impact velocities, where capillary forces around the periphery of a spreading droplet controlled droplet spreading. Berg, Ulrich and Schulte [12] photographed the impact of droplets of several metals including tin, lead, copper and steel to determine conditions under which the droplets splashed, breaking up on impact. Sobolev and Guilemany [13] developed analytical models to predict the shape and size of splats formed by droplets flattening out following impact.

Thermal contact resistance between a surface and an impinging molten droplet has been estimated by either measuring the substrate temperature variation [14], or the cooling rate of a molten drop after it spread on a metallic substrate [15,16]. However, in all these investigations the response time of the temperature sensors was much longer than the time taken for a droplet to spread during impact, so that their measurements are not applicable to the instant of initial impact on the surface. Amon et al. [17] used a calorimetric technique to measure the temperature of molten steel droplets, and developed a model to predict whether remelting of the substrate would occur when they were deposited on a steel surface.

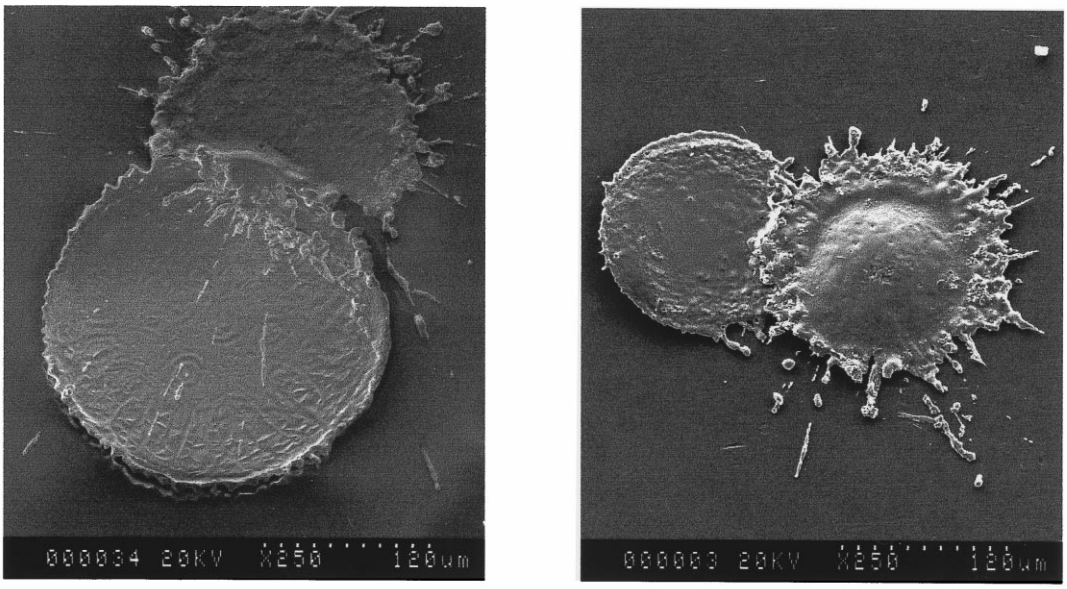

Fig. 1. Splats formed by the sequential impact of two nickel droplets (61 μm average diameter) with a velocity of 48 m/s on (a) a glass surface at 356°C, and (b) a polished stainless steel surface at 368°C.

In earlier publications [18,19] we presented a numerical model of droplet impact and solidification, and compared photographs of water and tin droplets impacting on a stainless steel surface with model predictions. In the present paper, we describe a much more extensive experimental investigation of molten metal droplet impact, including the effect of varying substrate temperature and impact velocity. We photographed the impact of 2.7 mm diameter tin droplets on a stainless steel surface. Droplet impact velocity was varied from 1.0 to 4.0 m/s and the substrate temperature from 25 to 240°C (above the melting point of tin, 232°C). We photographed droplet impact and measured the splat diameter and liquid–solid contact angle from these photographs. Droplets showed a range of behaviour, including spreading, recoil, and splashing. Variation in substrate temperature under the impacting droplet was measured using a fast response thermocouple, and thermal contact resistance between the droplet and substrate calculated by matching measured surface temperature variation with an analytical solution of heat conduction in the substrate. Our principal objective was to develop a simple model that can predict splat size, and determine when solidifi-

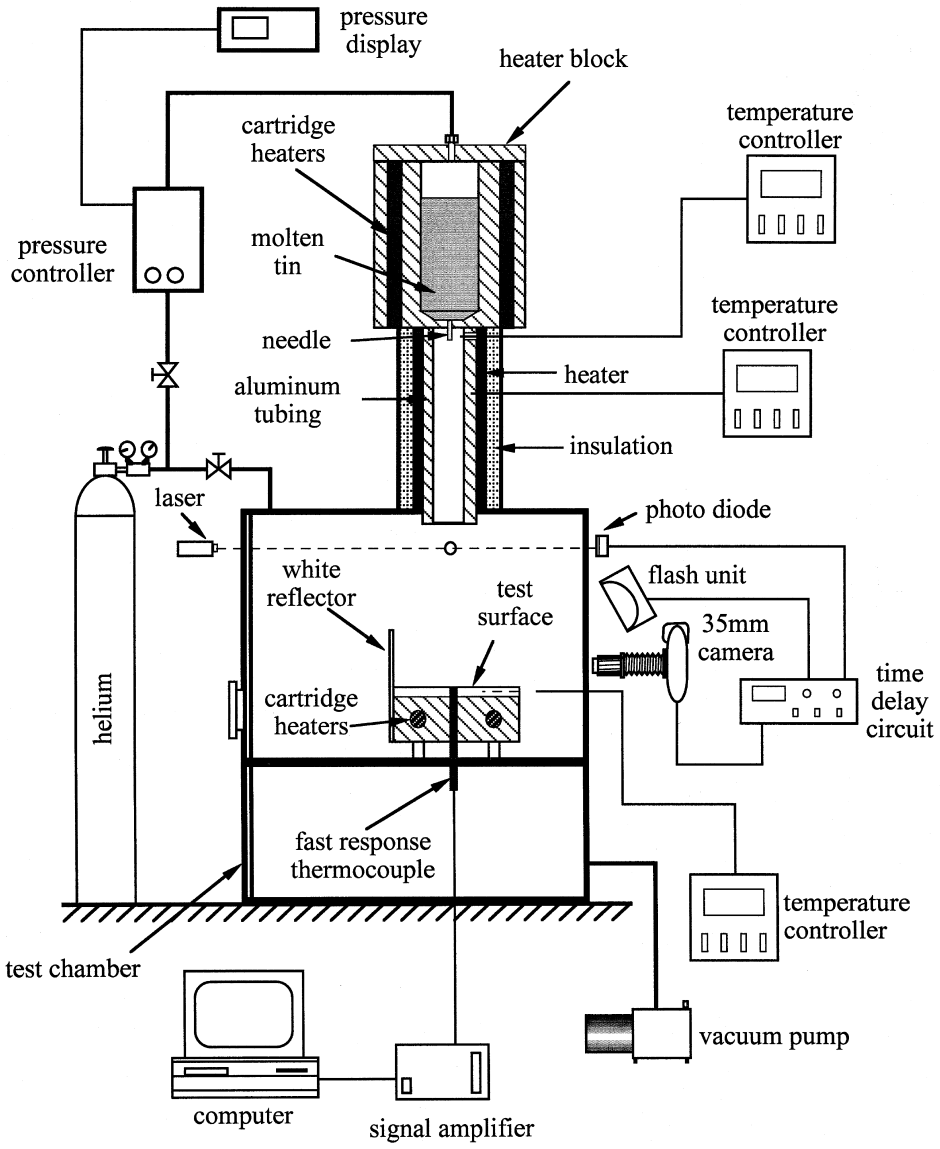

Fig. 2. Schematic diagram of the experimental apparatus.

cation would influence droplet impact dynamics. The model allows us to scale information obtained from laboratory experiments with large (2–3 mm) droplets to the small (10–100 μm) droplets typically found in thermal sprays.

2. Experimental method

Fig. 2 illustrates the experimental apparatus used. The main components were the droplet generator, a test surface on which the droplet landed, photography equipment and temperature measurement instrumentation. The droplet generator consisted of a 76.2 mm diameter by 76.2 mm long stainless steel cylinder, in which was machined a cavity 38.1 mm in diameter and 60.3 mm deep. The cylnder was heated by four 100 W cartridge heaters inserted into it which were regulated by a temperature controller (CN9112A, Omega Engineering, Stamford, CT). The cavity was filled with tin pellets (99.8% purity, Aldrich, Milwaukee, WI) and maintained at a temperature of approximately 240°C, which is above the melting point of tin ($T_m = 232$°C). The space above the molten tin was filled with helium, whose pressure was regulated by an electronic pressure controller (IP310D-020, Omega Engineering, Stamford, CT). Droplets were formed by increasing the gas pressure to 20–50 kPa above atmospheric, forcing molten tin through a 12 mm long stainless steel tube (with outer diameter 1.59 mm and inner diameter 0.508 mm) inserted through the bottom of the cavity. The tube was crimped 4 mm above the bottom end, forming a constriction that severed the column of molten tin flowing through it, allowing a single droplet to detach.

Droplets fell after detachment through a 25.4 mm diameter aluminium tube which was heated using a 125 W rope heater. The tube temperature was selected on the basis of heat loss calculations [20], so as to ensure that the droplet temperature at the instant of impact was 236°C. Droplets landed on the test surface, which was a 50.8 mm square by 6.35 mm thick stainless steel plate polished with 600 grit emery cloth. The test surface was mounted on a copper block heated by two 125 W cartridge. The droplet generator was mounted on a frame whose height above the test surface could be adjusted, allowing droplet impact velocity to be varied from 1 to 4 m/s. The test surface was housed in an acrylic desiccator (0.3 m × 0.3 m × 0.3 m in size) that was first evacuated with a vacuum pump and then filled with helium, preventing oxidation of tin droplets.

A single-shot photographic technique (similar to that described by Pasandideh-Fard et al. [19]) was used to capture droplet impact. As a droplet fell to the surface it passed through the beam of a helium–neon laser which was directed onto a photo diode. Interruption of the laser beam decreased the output voltage of the photo diode, which was detected by a timing circuit. The timing circuit opened the shutter of a Nikon F3 camera and started a time delay circuit with a 1 μs resolution. After a pre-set time had elapsed the time delay circuit sent a signal to trigger an electronic flash with a 8 μs flash duration (GR 1538-A, GenRad, Concord, MA), taking a single 35 mm photograph of an impacting droplet. Adjusting the time delay allowed photographs to be captured at different stages of droplet deformation, and the entire impact was pieced together from this sequence of photographs.

Measurements of the droplet spread diameter during deformation were made directly from 35 mm negatives by projecting the images onto a white surface using a photographic enlarger. The resolution of the droplet diameter measurements was ±0.01 mm. Contact angle measurements were also made from photographs, with a resolution estimated to be ±3°.

Surface temperature variation during droplet impact was recorded using a chromel–alumel (type K) thermocouple (E12-3-K-Style 7, Nanmac, Framingham, MA) which has a response time of 10 μs, as measured by the manufacturer. The thermocouple consists of fine ribbons of chromel and alumel, separated by an insulating layer of mica, enclosed in a stainless steel sheath. The thermocouple was inserted vertically through the stainless steel substrate (see Fig. 2) and ground flush with the test surface, forming a bare thermocouple junction on the surface at the point of impact of the droplet. Since the thermocouple does not protrude above the surface we do not expect it to influence fluid flow during droplet deposition. The signal from the thermocouple during droplet impact was amplified and recorded on a computer equipped with a data acquisition board.

3. Results and discussion

3.1. Droplet impact dynamics

Fig. 3 consists of three series of photographs showing molten tin droplets landing with velocity $V_o = 2.0$ m/s on a stainless steel surface maintained at temperatures of 25°C (Fig. 3a), 150°C (Fig. 3b) and 240°C (Fig. 3c), respectively. Each row of pictures in Fig. 3 shows successive stages of droplet deformation, with the time (t) from initial impact indicated. The reflection of the droplet is visible in the polished steel surface.

A droplet landing on a surface with initial temperature $T_{w,i} = 25$°C (Fig. 3a) spread into the shape of a flattened disk after impact and reaching its maximum

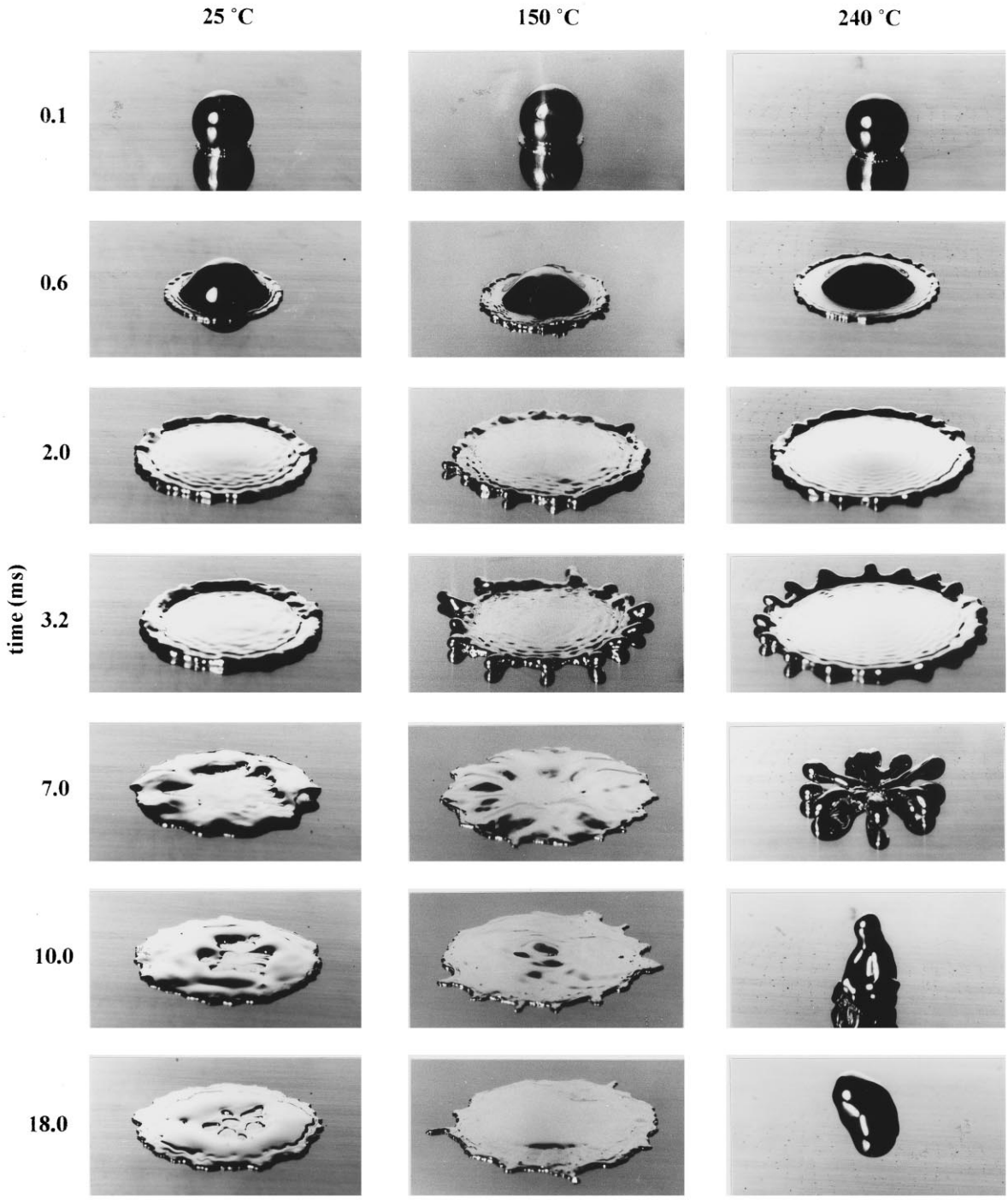

Fig. 3. Impact of molten tin droplets with velocity 2.0 m/s on a stainless steel surface at temperature (a) 25°C, (b) 150°C and (c) 240°C.

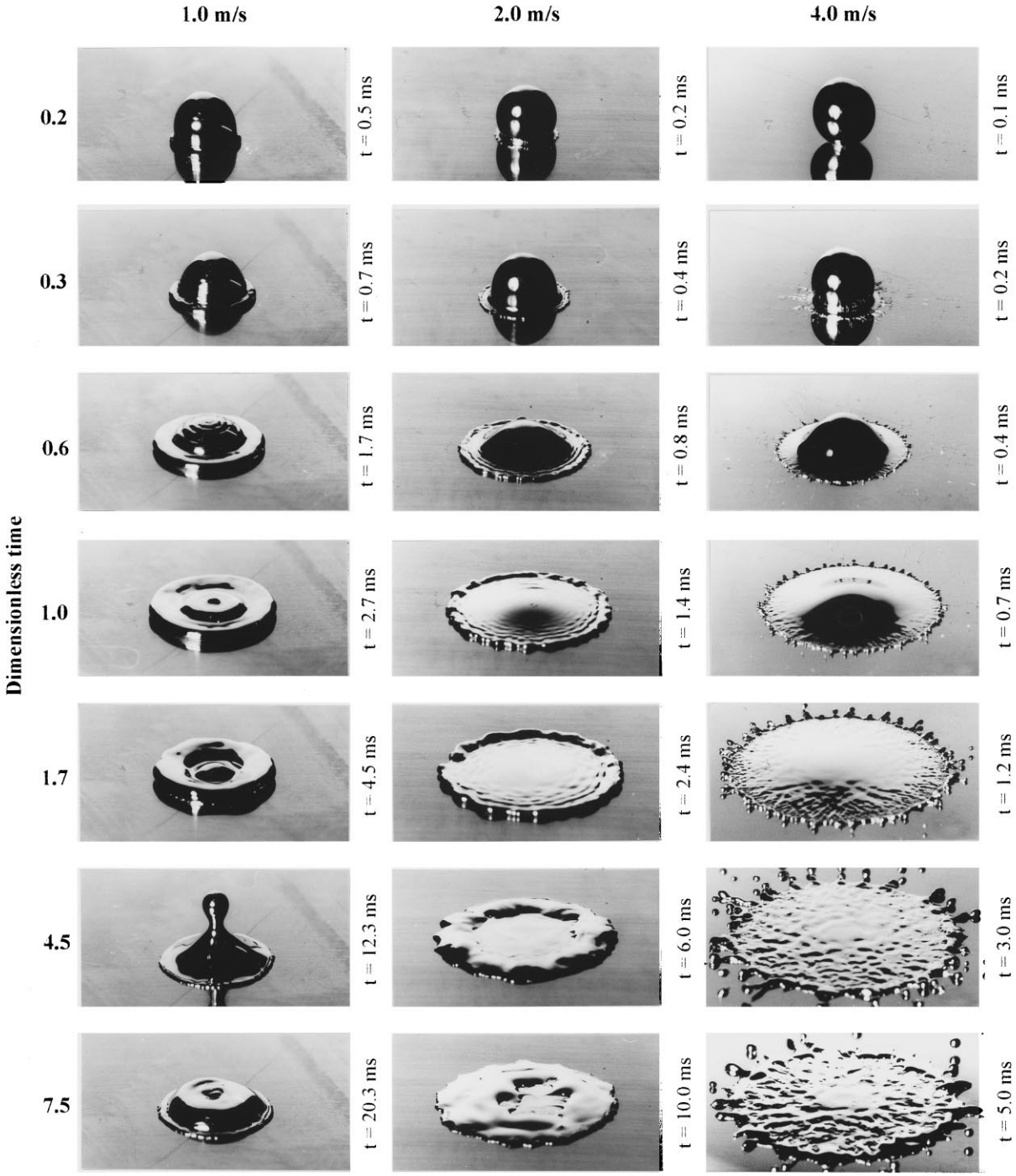

Fig. 4. Impact of molten tin droplets on a stainless steel surface at temperature 25°C with velocity (a) 1 m/s, (b) 2 m/s and (c) 4 m/s.

spread at approximately $t = 3.2$ ms. The edges of the droplet solidified by $t = 7$ ms, evident from the irregular shape of the splat. However, a film of liquid metal remained above the solidified layer which was pulled back by surface tension forces towards the center of the splat. Solidification was complete by $t = 18$ ms and no changes were seen in the splat shape after this time. The surface of the splat remained irregular, with craters left in it.

Solidification was slower for a drop landing on a surface at 150°C (Fig. 3b) than it had been with $T_{w,i} = 25$°C, and the drop spread further. The edges of the splat became unstable, resulting in the formation of fingers around the periphery of the drop. The fingers became larger ($t = 3.2$ ms) until further growth was arrested by solidification of the splat. Surface tension forces pulled the remaining liquid towards the centre of the drop. The final splat shape was much smoother than that observed at $T_{w,i} = 25$°C because freezing was less rapid and the liquid had more time to spread ($t = 18$ ms).

The temperature of a surface at 240°C (Fig. 3c) was well above the melting point of tin ($T_m = 232$°C) and close to the initial droplet temperature ($T_d = 236$°C); impact was therefore essentially isothermal and the droplet remained liquid. The maximum spread diameter of the droplet was larger ($t = 3.2$ ms) than it had been on a cold surface. The fingers were allowed to develop fully and grew towards the centre of the splat ($t = 7.0$ ms). Surface tension forces then pulled the droplet back together, eventually making it recoil off the surface ($t = 18.0$ ms).

The effect of increasing droplet velocity on impact dynamics is visible in Fig. 4, which hows droplets landing on a 25°C substrate with impact velocities of 1 m/s (Fig. 4a), 2 m/s Fig. 4b), and 4 m/s (Fig. 4c). Each row in Fig. 4 represents the same dimensionless time $t^* = tV_o/D_o$; the real time (t) from the instant of impact is indicated next to each frame. At a low impact velocity $V_o = 1$ m/s (Fig. 4a), the droplet reached its maximum spread a little after $t^* = 1.0$. The molten layer was pulled back by surface tension, and recoiled above the surface ($t^* = 4.5$). The drop finally subsided and solidified to form a rounded splat ($t^* = 7.5$). Increasing the impact velocity to 2 m/s (Fig. 4b) increased the splat diameter and reduced the splat thickness. The recoil of the droplet was also greatly diminished, so that there was only a small flow of liquid back from the edges of the splat towards its centre. There was also evidence of the formation of fingers around the edges of the splat ($t^* = 1.0$). At the highest velocity in our tests, 4 m/s (Fig. 4c), the fingers were large, and visible very early during impact. The tips of the fingers had enough inertia to detach as small satellite droplets ($t^* = 4.5$). The growth of the fingers was stopped by the droplet solidifying so that the final splat shape was reached by approximately $t^* = 4.5$, with little change after that time. No recoil was visible for $V_o = 4$ m/s.

The extent of droplet spread was quantified by measuring the splat diameter (D) from photographs and normalizing it by the initial droplet diameter (D_o) to give the "spread factor" ($\xi = D/D_o$). Fig. 5 shows the variation of spread factor during droplet impact on a surface at 25°C for impact velocities from 1–4 m/s. The maximum spread factor reached during impact (ξ_{max}) increased with impact velocity. Also, the dimensionless time required for a droplet to spread to its maximum extent (t_c^*) increased with impact velocity. Pasandideh-Fard et al. [18] used a simple model of droplet spread to estimate $t_c^* = 2.67$, irrespective of impact velocity. This value offers a reasonable order-of-magnitude estimate of the spreading time in our experiment (see Fig. 5).

Fig. 6 shows the evolution of spread factor for droplets impacting on a surface at 240°C, in which there was no solidification. The maximum spread factor at a given velocity was significantly larger than it was for droplets landing on a surface at 25°C, because spreading was not restrained by droplet freezing. Again, t_c^* increased with droplet velocity, but $t_c^* = 2.67$ was a reasonable average value. Once ξ reached a maximum value it began to decrease as droplets recoiled off the surface. Droplet recoil was pronounced in all cases with the droplet lifting completely off the surface (corresponding to $\xi = 0$).

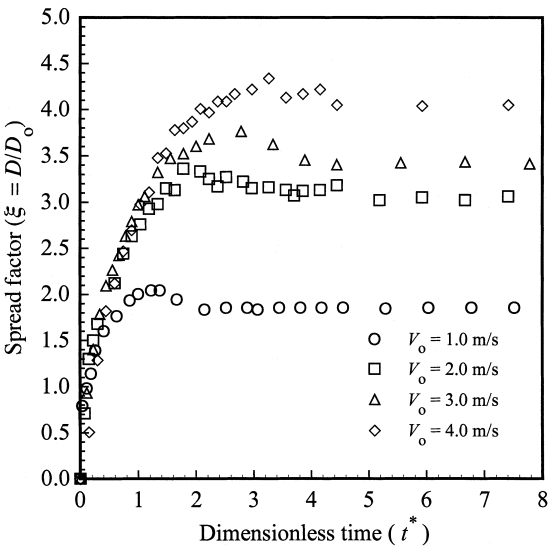

Fig. 5. Spread factor evolution for tin droplets impacting a stainless steel surface at 25°C with impact velocity V_o.

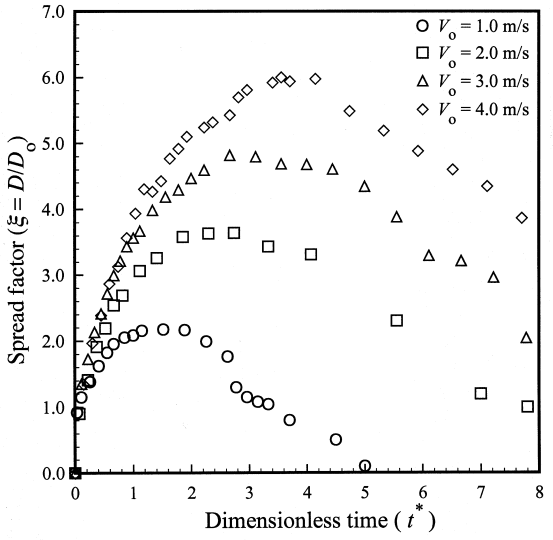

Fig. 6. Spread factor evolution for tin droplets impacting a stainless steel surface at 240°C with impact velocity V_o.

3.2. Thermal contact resistance

When a molten drop impinges on a cold substrate air pockets may be trapped at the interface between the two, offering resistance to heat transfer. This resistance increases as the droplet solidifies, because contact between two solid surfaces is poorer than that between a liquid and a solid. Previous estimates [14–16] of thermal contact resistance typically range between 10^{-4} and 10^{-5} m^2 K/W. However, these estimates were based on temperature measurements made with relatively slow sensors, with response times longer than the duration of droplet spreading. Thermal contact resistance during impact, before the droplet is completely solidified, would be expected to be smaller.

Fig. 7 shows the measured variation in temperature of the stainless steel surface during the impact of a tin droplet with a velocity of 4.0 m/s, for five initial surface temperatures: $T_{w,i} = 25$°C, 50°C, 100°C, 150°C and 200°C. The increase in surface temperature is plotted ($\Delta T = T_w - T_{w,i}$, where T_w is the surface temperature and $T_{w,i}$ the initial surface temperature), with $t = 0$ corresponding to the instant of droplet impact. Surface temperatures increased and reached a maximum within 1 ms of impact. The surface then began to cool, with the cooling occurring earlier at lower surface temperatures. Similar measurements were done at lower droplet impact velocities. The results are summarised in Fig. 8, where we used the maximum increase in surface temperature (ΔT_{max}, see Fig. 7) as a measure of droplet to surface heat transfer. ΔT_{max} increased slightly with impact velocity, indicating improved heat transfer. This may be because of increased forced convection, and also because molten metal fills in substrate roughness better when impinging at higher velocity, reducing the amount of gas trapped in pores at the droplet–substrate interface and decreasing thermal contact resistance. The effect was small, and could not be discerned for higher initial surface temperatures.

Previous studies [21] have used the so-called contact

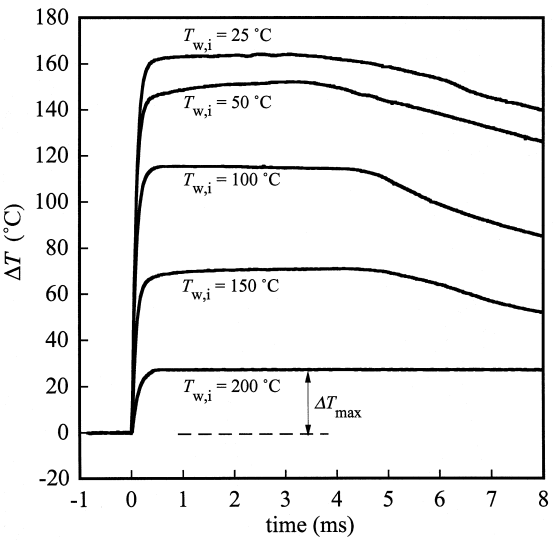

Fig. 7. Temperature variation of a stainless steel surface (initial surface temperatures $T_{w,i}$) during the impact of a tin droplet with velocity 4.0 m/s.

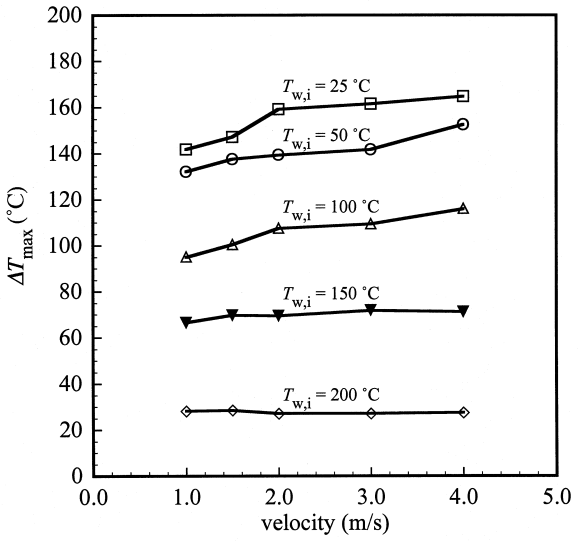

Fig. 8. Maximum increase in surface temperature for a tin droplet landing on a stainless steel surface at initial surface temperatures $T_{w,i}$.

temperature to predict the surface temperature under an impacting droplet. This is the temperature at the interface between two sem-infinite solid bodies suddenly brought into contact, with no contact resistance between them, and is given by:

$$T_w = \frac{\sqrt{\gamma_w}T_{w,i} + \sqrt{\gamma_d}T_d}{\sqrt{\gamma_w} + \sqrt{\gamma_d}} \quad (1)$$

where $\gamma = k\rho C$. Comparing predictions from Eq. (1) with experimental results showed that calculated temperature rise was much less than that measured. We concluded that convection effects, which are not included in Eq. (1), are significant during the early stages of droplet impact (e.g., $t^* < 1$), when there is a constant flow of fresh fluid brought to the surface by the spreading droplet. A more realistic assumption would be that the droplet temperature is constant during this time, equal to its initial temperature. Also, contact between the droplet and substrate would be imperfect because of air trapped at the interface, producing added resistance to heat transfer. We therefore modelled the substrate as a semi-infinite body initially at temperature $T_{w,i}$. At time $t = 0$ the droplet, at constant temperature T_d is brought in contact with the surface, with a thermal contact resistance R_c between them. If heat transfer is by one-dimensional heat conduction, the surface temperature variation is given by [22]:

$$T_w = T_{w,i} + (T_d - T_{w,i})\left\{1 - \exp\left(\frac{\alpha_w t}{R_c^2 k_w^2}\right)\mathrm{erfc}\left(\frac{\sqrt{\alpha_w t}}{R_c K_w}\right)\right\} \quad (2)$$

We selected the value of R_c by matching equation (2) to our experimental measurements using a least squares fit over $0 < t < 0.5$ ms. Fig. 9 shows typical curve fits for $T_{w,i} = 50°C$ and $V_o = 1$ m/s and 4 m/s. The measured temperature change was less than that predicted by theory for $t < 0.1$ ms, which may have been due to a lag in thermocouple measurement, which had a response time of 10 μs. The predicted interface temperature from Eq. (1) is also shown in Fig. 9, and is seen to be much lower than the measured value.

Calculated values of thermal contact resistance are summarised in Fig. 10, which shows the variation of R_c with impact velocity. We also confirmed that calculations of R_c were not very sensitive to uncertainties in temperature measurement or substrate property values. We calculated the change produced in R_c by a ±5% variation in surface properties k_w, ρ_w, and C_w, and a ±2°C variation in the initial droplet temperature (T_d) and the experimentally measured surface temperature data (T_w). Changes in R_c produced by each of these variations were then summed, to give the maximum cumulative error. Averages of these errors at each surface temperature are listed in Fig. 10.

Measured values of thermal contact resistance ranged between 10^{-6} and 5×10^{-6} m^2 K/W. These results agree well with those of Pasandideh-Fard et al. [19]

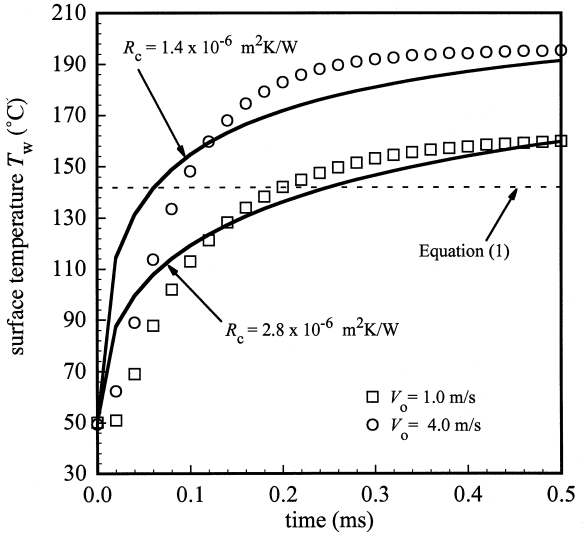

Fig. 9. Measured and calculated surface temperature variation during the impact of a tin droplet with velocity V_o on a stainless steel surface at 50°C.

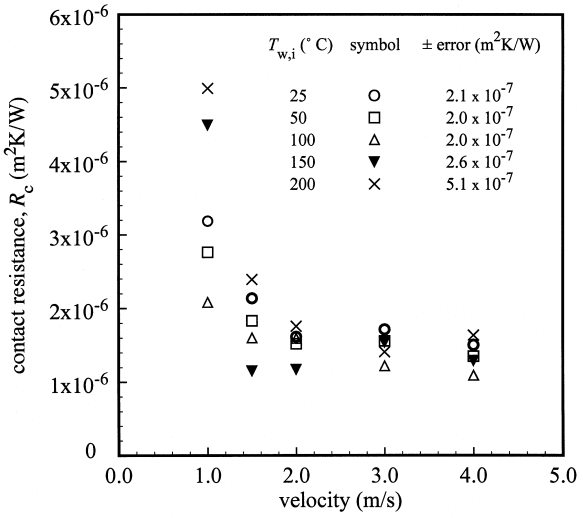

Fig. 10. Variation of contact resistance with impact velocity for a tin droplet impacting on a stainless steel surface initially at temperature $T_{w,i}$.

who, using a much more sophisticated numerical model of droplet impact, calculated $R_c = 10^{-6}$ m^2 K/W for a tin droplet impacting a surface with a velocity of 1.6 m/s. Thermal contact resistance was highest at low impact velocity, and reached a constant value of approximately 10^{-6} m^2 K/W for $V_o \geq 2$ m/s. For $R_c = 10^{-6}$ m^2 K/W, the Biot number ($Bi = D_o/(R_c k_d)$) is 85 suggesting that contact resistance will not affect droplet impact in our experiments. Ruhl [23] determined that the contact resistance does not affect drop deformation if $Bi > 30$.

3.3. Models of droplet spread and recoil

Pasandideh-Fard et al. [18,19] developed a simple model to predict the maximum spread diameter of an impacting droplet. In their model, they equated the energy before and after impact, accounting for the energy dissipation during impact. The initial kinetic energy (KE_1) and surface energy (SE_1) of a liquid droplet before impact are:

$$KE_1 = \left(\frac{1}{2}\rho V_o^2\right)\left(\frac{\pi}{6}D_o^3\right) \tag{3}$$

$$SE_1 = \pi D_o^2 \sigma \tag{4}$$

After impact, when the droplet is at its maximum extension, the kinetic energy is zero and the surface energy (SE_2) is:

$$SE_2 = \frac{\pi}{4}D_{max}^2\sigma(1-\cos\theta_a) \tag{5}$$

where θ_a is the advancing liquid–solid contact angle. The work done in deforming the droplet against viscosity (W) is [18]:

$$W = \frac{\pi}{3}\rho V_o^2 D_o D_{max}^2 \frac{1}{\sqrt{Re}} \tag{6}$$

in which Re is the Reynolds number $Re = V_o D_o/\nu$. The effect of solidification in restricting droplet spread is modelled by assuming that all the kinetic energy stored in the solidified layer is lost. If the solid layer has average thickness s and diameter d_s when the splat is at its maximum extension, then the loss of kinetic energy (ΔKE) is approximated by:

$$\Delta KE = \left(\frac{\pi}{4}d_s^2 s\right)\left(\frac{1}{2}\rho V_o^2\right) \tag{7}$$

d_s varies from 0 to D_{max} during droplet spread: a reasonable estimate of its mean value is $d_s \sim D_{max}/2$. Substituting Eqs. (3)–(7) into the energy balance $KE_1 + SE_1 = SE_2 + W + \Delta KE$ yields an expression for the maximum spread factor:

$$\xi_{max} = \frac{D_{max}}{D_o} = \sqrt{\frac{We+12}{\frac{3}{8}We s^* + 3(1-\cos\theta_a) + 4\frac{We}{\sqrt{Re}}}} \tag{8}$$

We is the Weber number ($We = \rho V_o^2 D_o/\sigma$) and s^* is the dimensionless solid layer thickness ($s^* = s/D_o$). For the case of isothermal droplet impact ($T_{w,i} = 240$°C) there is no solidification, $s^* = 0$, and Eq. (8) reduces to the simple model developed by Pasandideh-Fard et al. [18] for spread of a liquid drop:

$$\xi_{max} = \sqrt{\frac{We+12}{3(1-\cos\theta_a) + 4\left(\frac{We}{\sqrt{Re}}\right)}} \tag{9}$$

There are two unknowns in Eq. (8): advancing contact angle (θ_a) and solidified layer thickness (s^*). Liquid–solid contact angles during spreading and recoil of droplets were measured from enlarged photographs. The results are shown in Fig. 11, for two impact velocities (1 and 3 m/s) and two substrate temperatures (25 and 240°C). Impact velocities in the range of our experiments seemed to have little influence on contact angle. Droplets landing on a surface at 240°C did not solidify, and the molten tin was in contact with the stainless steel substrate during both spreading and recoil. The receding contact angle (measured during droplet recoil) was only slightly smaller than the advancing contact angle (measured during droplet spread). Defining a contact angle during impact on a surface at 25°C was more difficult, because the splat solidified as it spread so that during recoil the receding

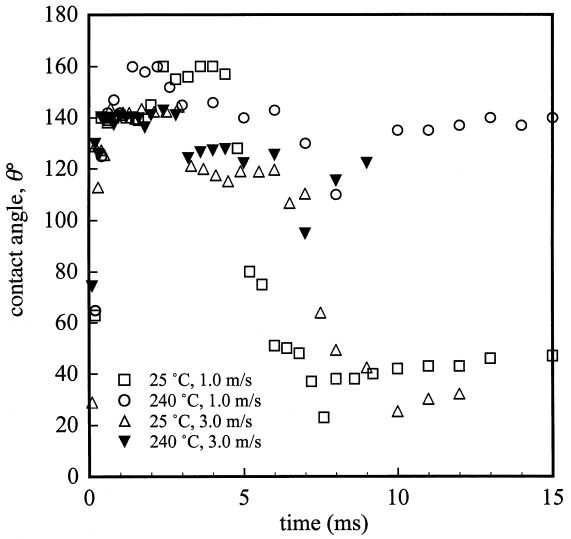

Fig. 11. Contact angle variation during impact of tin droplets on a stainless steel surface.

layer of molten tin was in contact with a frozen tin substrate (see Fig. 4a). The receding contact angle was therefore significantly smaller than the advancing contact angle. However, to calculate the maximum spread diameter only the value of the advancing contact angle value is needed, and a constant value of $\theta_a = 140^\circ$ was used for all our calculations.

The growth in thickness of the solidified layer was calculated using an approximate analytical solution developed by Poirier and Poirier [24]. Their model assumes that heat transfer is by 1D conduction; there is no thermal contact resistance at the droplet–substrate interface; the temperature drop across the solid layer is negligible; the substrate is semi-infinite in extent and has constant thermal properties. The dimensionless solidification thickness was expressed as a function of the Stefan number ($Ste = C(T_m - T_{w,i})/H_f$), Peclet number ($Pe = V_o D_o/\alpha$) and $\gamma = k\rho C$:

$$s^* = \frac{2}{\sqrt{\pi}} Ste \sqrt{\frac{t^* \gamma_w}{Pe \gamma_d}} \tag{10}$$

Substituting Eq. (10) into (8) gives the maximum spread of a droplet that is solidifying during impact:

$$\xi_{max} = \sqrt{\frac{We + 12}{WeSte\sqrt{\frac{3\gamma_w}{2\pi Pe\gamma_d}} + 3(1 - \cos\theta_a) + 4\left(\frac{We}{\sqrt{Re}}\right)}} \tag{11}$$

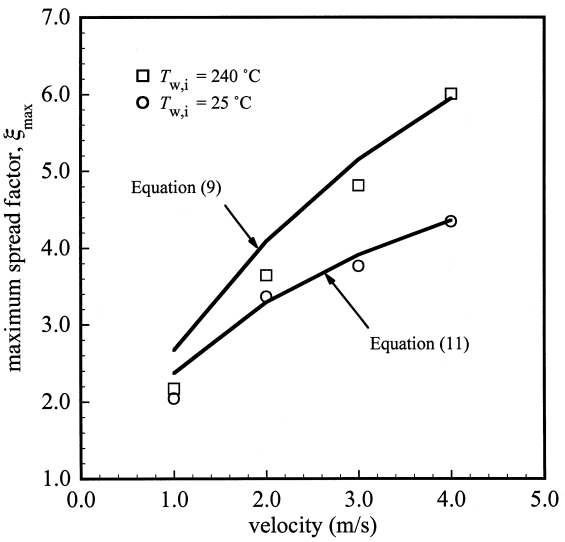

Fig. 12. Calculated (lines) and measured (symbols) variation of maximum spread factor with impact velocity for a tin droplet impacting a stainless steel surface at surface temperature $T_{w,i}$.

The variation of ξ_{max} with impact velocity predicted by Eq. (11) for droplets falling on a substrate at 25°C is shown in Fig. 12, along with measured values. Predictions of ξ_{max} from Eq. (9), for a droplet spreading without solidifying, are also compared with measurements for droplets impacting a surface at 240°C. Agreement between measured and calculated values is good in both instances. At low impact velocity we predicted somewhat larger values of ξ_{max} than were measured: to estimate viscous dissipation the model assumes that there exists a thin boundary layer in the drop [18], which is not true when the droplet is deposited very gently.

It was gratifying to find that the splat diameter of particles in a thermal spray can be predicted with reasonable accuracy using Eq. (11). For example, for the nickel particles shown in Fig. 1, we calculated $Re = 4370$, $We = 624$, $Ste = 1.554$ and $Pe = 228$. The term involving contact angle θ_a is small in comparison to the others in the denominator and was neglected. Calculated values of ξ_{max} were 2.9 on a stainless steel substrate (measured $\xi_{max} = 2.4$) and 3.4 on a glass substrate (measured $\xi_{max} = 3.2$).

Though the model can be used to estimate the maximum splat diameter, it cannot predict features controlled by the dynamics of liquid spreading, such as freezing around the droplet edge or droplet splashing. However, it is useful in estimating the relative importance of forces controlling fluid motion. The three terms in the denominator of the right-hand side of Eq. (11) represent the three effects that restrain droplet spreading: solidification, surface tension, and viscous dissipation respectively. For thermal spray particles, surface tension effects are negligible. Comparing the relative magnitude of the other two terms, solidification effects are negligible if:

$$\Phi = \frac{Ste}{\sqrt{Pr}} \sqrt{\frac{\gamma_w}{\gamma_d}} < 1 \tag{12}$$

where we have defined a "solidification parameter", Φ and the Prandtl number $Pr = Pe/Re = \nu/\alpha$. For nickel droplets plasma sprayed onto a steel surface $\Phi = 5.1$ and solidification plays an important role in restricting spread. We observed that nickel particles froze during impact on a stainless steel surface before spreading was complete (see Fig. 1b). For the same particle deposited on a glass surface $\Phi = 0.8$ and solidification is much slower; the particles flattened completely before freezing (Fig. 1a).

The effect of solidification in restricting droplet spread becomes more pronounced as droplet impact velocity increases (see Fig. 12). This seems counter-intuitive at first: faster droplets spread more quickly, reducing the time available for solidification. It is true that as impact velocity increases the thickness of the

solidified layer becomes less; s^* decreased by a factor of two when V_o increases from 1.0 to 4.0 m/s. However, the splat diameter increases, so that the total volume of tin that freezes during impact increases. We can quantify this effect by normalising the energy terms (Eq. (5)–(7)) with the initial droplet energy ($SE_1 + KE_1$). The normalised surface energy (ψ_{SE_2}) is:

$$\psi_{SE_2} = \frac{SE_2}{SE_1 + KE_1} = \left(1 + \frac{Wes^*}{8(1-\cos\theta_a)} + \frac{4}{3}\frac{We}{(1-\cos\theta_a)\sqrt{Re}}\right)^{-1} \quad (13)$$

the normalised viscous energy dissipation (ψ_w) is:

$$\psi_W = \frac{W}{SE_1 + KE_1} = \left(1 + \frac{3}{32}\sqrt{Re}s^* + \frac{3}{4}\frac{\sqrt{Re}(1-\cos\theta_a)}{We}\right)^{-1} \quad (14)$$

and normalised energy loss due to solidification ($\psi_{\Delta KE}$):

$$\psi_{\Delta KE} = \frac{\Delta KE}{SE_1 + KE_1} = \left(1 + \frac{8(1-\cos\theta_a)}{Wes^*} + \frac{32}{3}\frac{1}{s^*\sqrt{Re}}\right)^{-1} \quad (15)$$

Fig. 13 shows the variation of these normalised energies with impact velocity for droplets impacting on a surface at 25°C. In all cases s^* was evaluated from Eq. (10) at $t^* = 2.67$, when droplets were at their maximum extension [18]. The energy lost to solidification ($\psi_{\Delta KE}$) is seen to increase with impact velocity, resulting in smaller splat sizes.

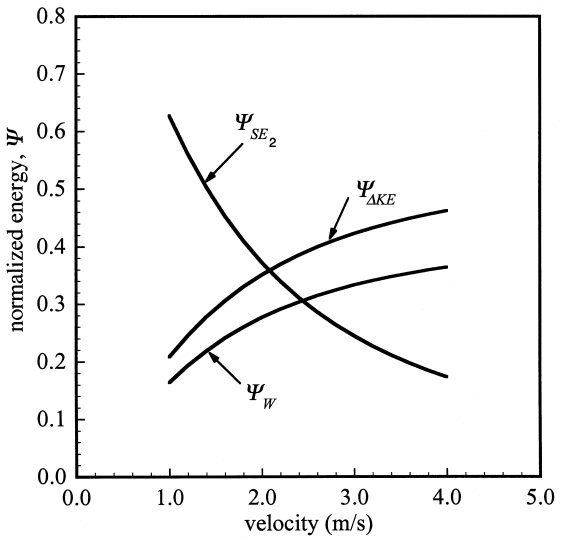

Fig. 13. Calculated normalised surface energy, work done and loss of kinetic energy due to solidification, as a function of droplet impact velocity.

The phenomenon of droplet recoil can also be understood with the help of Fig. 13. Droplets recoiled off the surface after impacting at low velocity (see Fig. 4a). As impact velocity increased, the height of recoil decreased (Fig. 4c). Recoil is caused by surface tension pulling the droplet back. Increasing impact velocity increases the work done against viscosity (ψ_W, see Fig. 13) and reduces the amount of surface energy that remains (ψ_{SE_2}), decreasing the height of recoil. Droplet rebound was even more pronounced when there was no solidification. Fig. 14 shows the impact of a droplet on a surface at 240°C with a velocity of 1 m/s. In this case no energy was lost because of freezing of tin and surface energy was sufficient to lift the droplet completely off the surface.

3.4. Droplet splashing

Increasing impact velocity also leads to an increase in the number and size of fingers formed around the periphery of the drop. For droplets impacting on a cold surface the growth of the fingers was arrested by freezing (see Fig. 4). However, in the absence of solidification the fingers grew larger and led to break-up of the droplet. Fig. 15 shows photographs of the impact of a droplet with a velocity of 4 m/s on a surface at 240°C. Fingers were seen to form in the earliest frame ($t = 0.2$ ms). They grew larger and their tips began to break off to form small satellite droplets. The splat reached its maximum extension ($t = 2.9$ ms) and then began to recede. The fingers of liquid merged with each other as the splat became smaller. Finally, the small droplet that remained recoiled off the surface ($t = 12.1$ ms).

The number of fingers formed around the droplet increased with impact velocity. Fig. 16 shows the variation of the number of fingers during the spread and recoil of a drop falling on a surface at 240°C, for impact velocities of 2, 3 and 4 m/s. The amplitude of waves formed around a drop impacting at 1 m/s was too small for them to be counted accurately (see Fig. 14). The number of fingers remained approximately constant during droplet spread ($t^* < 2.7$), and then decreased as the droplet recoiled and fingers coalesced with each other.

Mundo et al. [25] and Stow and Hadfield [26] studied the splashing of liquid droplets. From experiments they concluded that splashing occurred when the "splash parameter" $K = \sqrt{We\sqrt{Re}}$ exceeded a critical value. Allen [27] suggested that fingers form around the periphery of a spreading droplet because of a Ray-

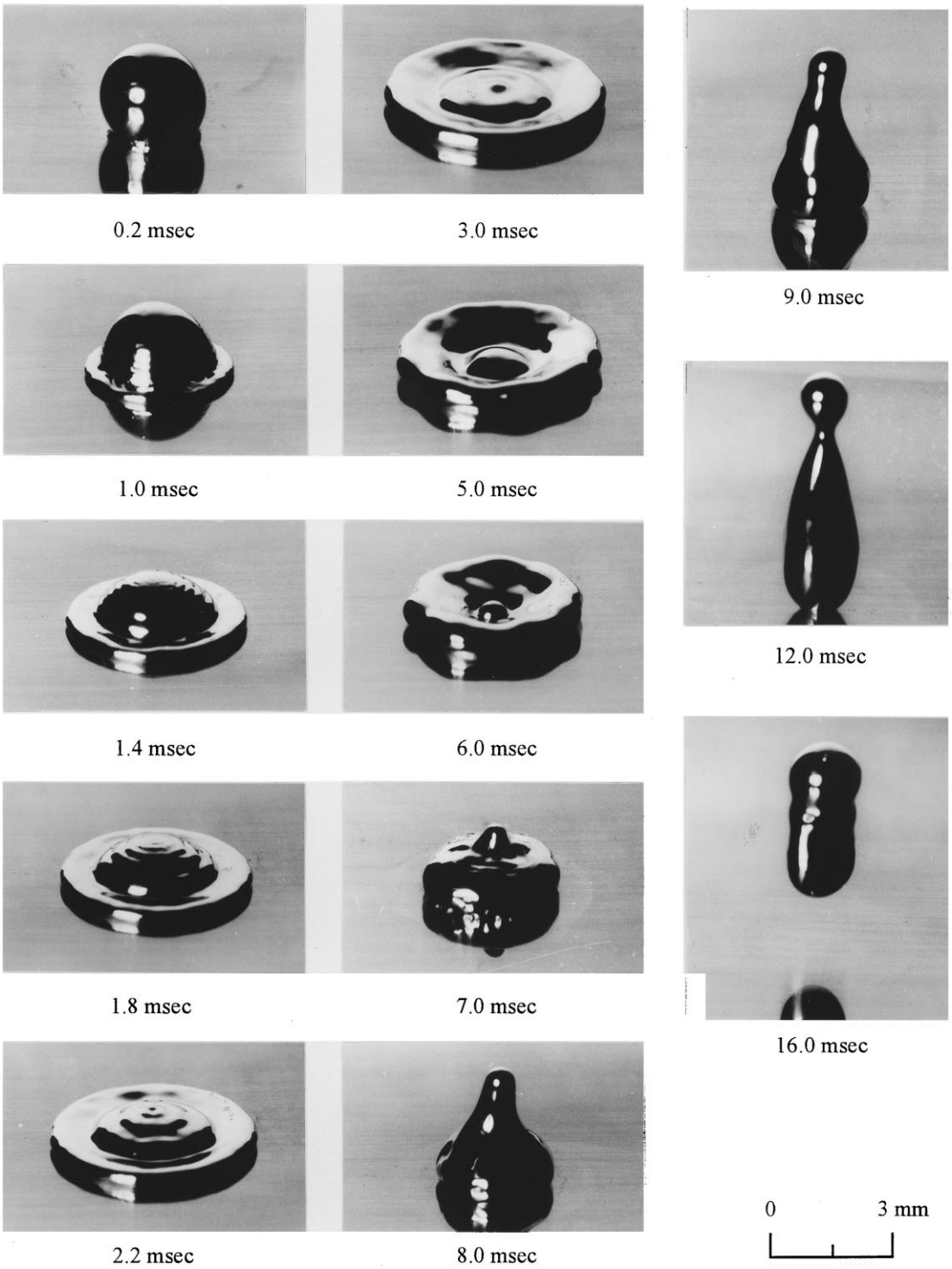

Fig. 14. Impact of a molten tin droplet with velocity 1 m/s on a stainless steel surface at temperature 240°C.

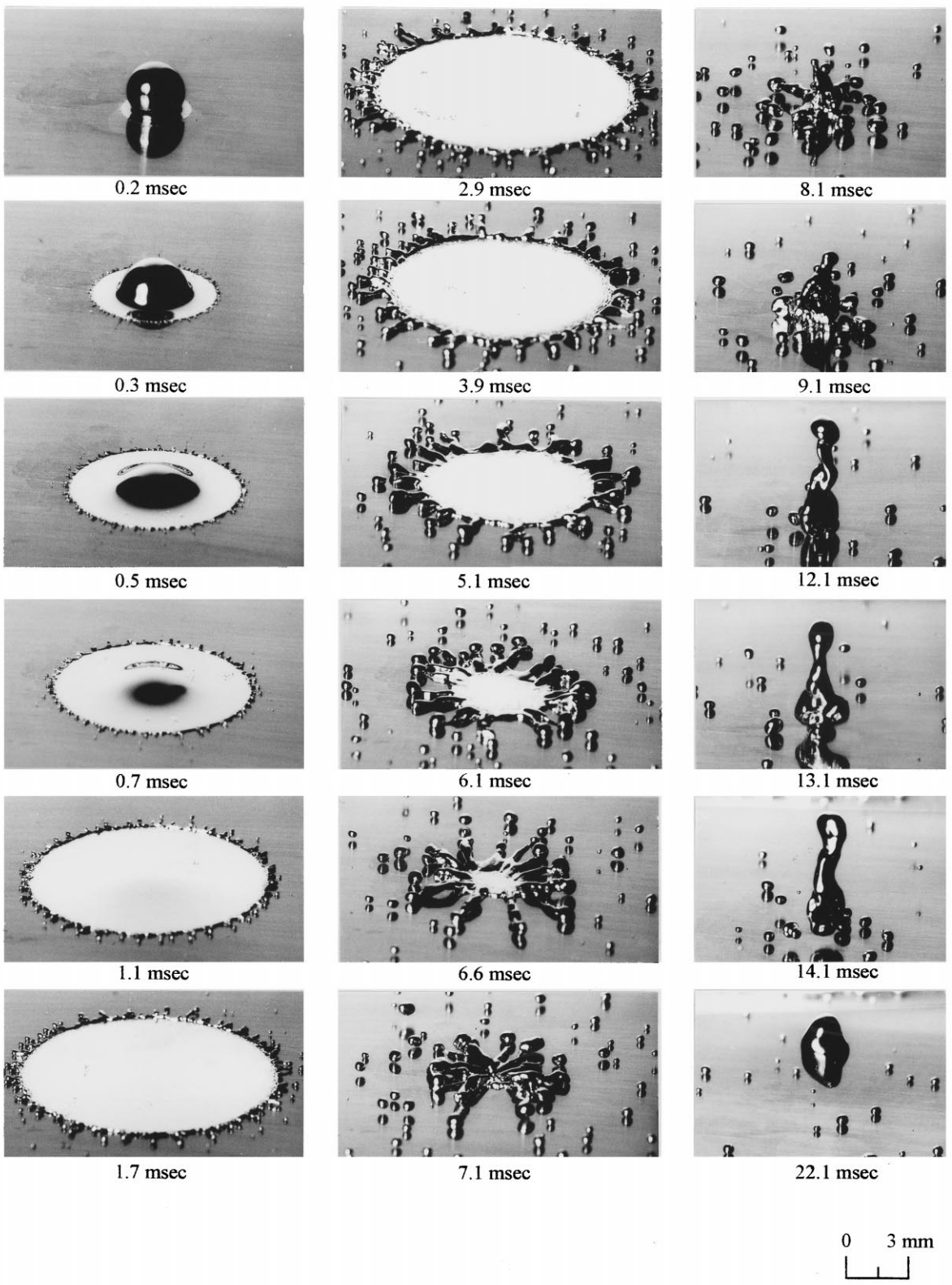

Fig. 15. Splashing of a molten tin droplet during impact with velocity 4 m/s on a stainless steel surface at temperature 240°C.

leigh–Taylor instability, which is caused by the acceleration of the interface between two fluids of different density. If the magnitude of acceleration is a, the wavelength of the interfacial waves is [27]

$$\lambda = 2\pi\sqrt{\frac{3\sigma}{a\rho}} \tag{16}$$

The number of waves (N) around the perimeter of the drop equals:

$$N = \frac{\pi D_{\max}}{\lambda} = D_{\max}\sqrt{\frac{a\rho}{12\sigma}} \tag{17}$$

A simple estimate of the acceleration of the tip of the spreading liquid jet is $a \sim V_o^2/D_o$. Substituting in Eq. (17) gives:

$$N = \xi_{\max}\sqrt{\frac{We}{12}} \tag{18}$$

$\xi_{\max}$ can be estimated from Eq. (9). Typically, at velocities large enough to produce splashing, $We/\sqrt{Re} \gg 1$ and $We \gg 12$, so that Eq. (9) reduces to:

$$\xi_{\max} = \frac{Re^{1/4}}{2} \tag{19}$$

Substituting the above expressions for $\xi_{\max}$ into Eq. (18) gives:

$$N = \sqrt{\frac{We\sqrt{Re}}{48}} = \frac{K}{4\sqrt{3}} \tag{20}$$

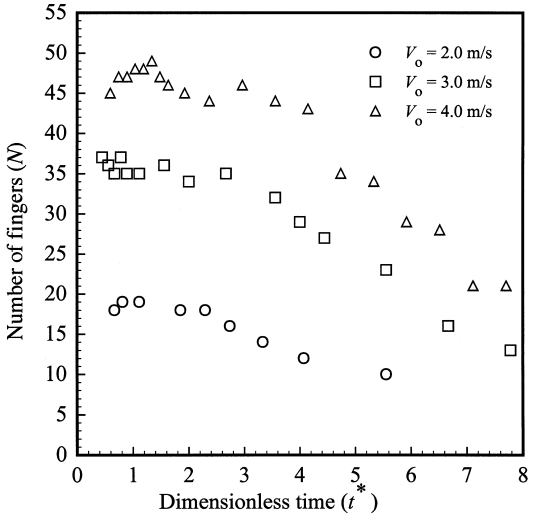

Fig. 16. Number of fingers formed around the circumference of a tin drop as it spreads after impinging with velocity V_o on a stainless steel surface at 240°C.

It is interesting that the simple analysis above shows the number of fingers to be a function of the splash parameter K, which had earlier been defined purely on an empirical basis [25,26]. The number of fingers around the circumference of a droplet at its maximum extension is shown in Fig. 17 as a function of impact velocity. Predictions from Eq. (20) are seen to agree well with experiments. Droplets impacting on a cold surface had fewer fingers forming around their periphery (Fig. 17). To predict the number of fingers, we substituted Eq. (11) in Eq. (18) to give

$$N = \sqrt{\left(\frac{We}{12}\right)\left(\frac{We+12}{WeSte\sqrt{\frac{3\gamma_w}{2\pi Pe\gamma_d}} + 3(1-\cos\theta_a) + 4\left(\frac{We}{\sqrt{Re}}\right)}\right)} \tag{21}$$

which included the effect of solidification on droplet spread. The results agreed well with measurements. This suggests that Eq. (16) offers a reasonable estimate of the wavelength of the fingers for impact on a surface at both 25 and 240°C. The difference in the number of fingers in the two cases is due to the difference in spread factors.

4. Conclusions

We studied the effect of varying impact velocity and substrate temperature during impact of molten tin droplets on a stainless steel plate. We photographed the deformation of impinging droplets and measured

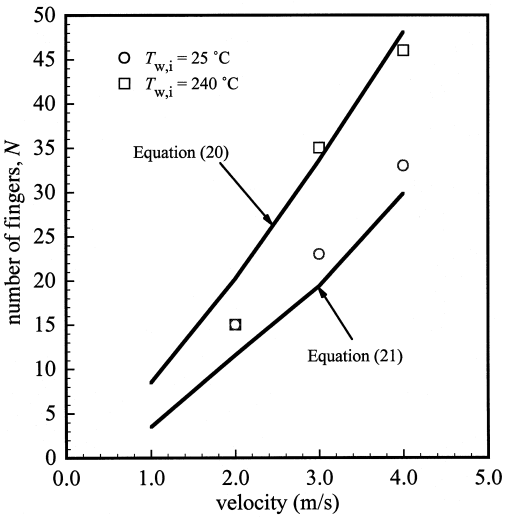

Fig. 17. Number of fingers formed around the circumference of a tin droplet at its maximum spread diameter.

surface temperature variation during impact. Contact resistance between the droplet and substrate was calculated from temperature measurements, and found to have negligible impact on droplet impact dynamics in our experiments. A simple energy conservation model was used to calculate the maximum spread factor; model predictions agreed well with experimental measurements. The model can also be used to define a solidification parameter Φ; solidification will have little influence on droplet spreading if $\Phi < 1$. We observed formation of fingers around the droplet periphery when impact velocity was increased. The number of fingers could be predicted assuming that their wavelength was that of a Rayleigh–Taylor instability.

References

[1] A.M. Worthington, A Study of Splashes, Longmans & Green, London, 1908.

[2] M. Varadelle, A. Varadelle, A.C. Leger, P. Fauchais, D. Gobin, Influence of particle parameters at impact on splat formation and solidification in plasma spraying process, Journal of Thermal Spraying Technology 4 (1) (1994) 50–58.

[3] V. Pershin, I. Thomson, S. Chandra, J. Mostaghimi, Nickel splat formation during plasma spraying, in: Proceedings of the 14th International Symposium on Plasma Chemistry, 1999, pp. 2089–2094.

[4] J. Madejski, Solidification of droplets on a cold surface, International Journal of Heat and Mass Transfer 19 (1976) 1009–1013.

[5] S. Inada, Transient heat transfer from a free-falling molten drop of lead to a cold plate, Journal of Chemical Engineering of Japan 21 (1988) 582–588.

[6] S. Inada, W.-J. Yang, Solidification of molten metal droplets impinging on a cold surface, Experimental Heat Transfer 7 (1994) 93–100.

[7] E.W. Collings, A.J. Markworth, J.K. McCoy, J.H. Saunders, Spalt-quench solidification of freely falling liquid-metal drops by impact on a planar substrate, Journal of Materials Science 25 (1990) 3677–3682.

[8] H. Fukanuma, A. Ohmori, Behavior of molten droplets impinging on flat surfaces, in: Proceedings of the 7th National Thermal Spray Conference, 1994, pp. 563–568.

[9] T. Watanabe, I. Kuribayashi, T. Honda, A. Kanzawa, Deformation and solidification of a droplet on a cold substrate, Chemical Engineering Science 47 (1992) 3059–3065.

[10] S. Schiffiano, A.A. Sonin, Motion and arrest of a molten contact line on a cold surface: an experimental study, Physics of Fluids 9 (1997) 2217–2226.

[11] S. Schiffiano, A.A. Sonin, Molten metal deposition and solidification at low Weber numbers, Physics of Fluids 9 (1997) 3172–3187.

[12] M. Berg, J. Ulrich, G. Schulte, Experimental determination of splashing thresholds of molten metal droplets impacting on solid and liquid surfaces, in: Proceedings of ILASS-Europe, 1998, pp. 371–373.

[13] V.V. Sobolev, J.M. Guilemany, Flattening of droplets and formation of splats in thermal spraying: a review of recent work—Part 1, Journal of Thermal Spray Technology 8 (1999) 87–101.

[14] T. Loulou, E.A. Artyukhin, J.P. Bardon, Solidification of molten tin drop on a nickel substrate, Heat Transfer 1994: Proceedings of the 10th International Heat Transfer Conference, Institution of Chemical Engineers, UK, 4 (1994) 73–78.

[15] W. Liu, G.X. Wang, E.F. Matthys, Thermal analysis and measurements for a molten metal drop impacting on a substrate: cooling, solidification and heat transfer coefficients, International Journal of Heat and Mass Transfer 38 (1995) 1387–1395.

[16] G.X. Wang, E.F. Matthys, Experimental investigation of interfacial thermal conductance for molten metal solidification on a substrate, Journal of Heat Transfer 118 (1996) 157–163.

[17] C.H. Amon, K.S. Schmaltz, R. Merz, F.B. Prinz, Numerical and experimental investigation of interface bonding via substrate remelting of an impinging molten metal droplet, Journal of Heat Transfer 118 (1996) 164–172.

[18] M. Pasandideh-Fard, Y.M. Qiao, S. Chandra, J. Mostaghimi, Capillary effects during droplet impact on a solid surface, Physics of Fluids 8 (1996) 650–659.

[19] M. Pasandideh-Fard, R. Bhola, S. Chandra, J. Mostaghimi, Deposition of tin droplets on a steel plate: simulations and experiments, International Journal of Heat and Mass Transfer 41 (1998) 2929–2945.

[20] S.D. Aziz, Impact velocity and surface temperature effects on the collision of a molten tin droplet on a solid surface, M.A.Sc. thesis, University of Toronto, August 1998.

[21] Y.M. Qiao, S. Chandra, Boiling of droplets on a hot surface in low gravity, International Journal of Heat and Mass Transfer 39 (1996) 1379–1393.

[22] H.S. Carslaw, J.C. Jaeger, Conduction of Heat in Solids, in: Oxford University Press, London, 1959, pp. 88–89.

[23] R.C. Ruhl, Cooling rates in splat cooling, Materials Science and Engineering 1 (1967) 313–320.

[24] D.R. Poirier, E.J. Poirier, Heat Transfer Fundamentals for Metal Casting, 2nd ed., Minerals, Metals and Materials Society, Warrendale, PA, 1994, pp. 41–42.

[25] C. Mundo, M. Sommerfeld, C. Tropea, Droplet–wall collisions: experimental studies of the deformation and break up process, International Journal of Multiphase Flow 21 (1995) 151–173.

[26] C.D. Stow, M.G. Hadfield, An experimental investigation of fluid flow resulting from the impact of a water drop with an unyielding surface, Proceedings of the Royal Society A 373 (1981) 419–441.

[27] R.F. Allen, The role of surface tension in splashing, Journal of Colloid and Interface Science 51 (1975) 350–351.